Analysis of wave propagation in a two-dimensional photonic crystal with negative index of refraction: plane wave decomposition of the Bloch modes

Alejandro Martínez, Hernán Míguez, José Sánchez-Dehesa, and Javier Martí

Valencia Nanophotonics Technology Center, Universidad Politécnica de Valencia
Camino de Vera s/n, 46022, Valencia (Spain)
almarab@ntc.upv.es

Abstract: This work presents a comprehensive analysis of electromagnetic wave propagation inside a two-dimensional photonic crystal in a spectral region in which the crystal behaves as an effective medium to which a negative effective index of refraction can be associated. It is obtained that the main plane wave component of the Bloch mode that propagates inside the photonic crystal has its wave vector $\vec{k}'$ out of the first Brillouin zone and it is parallel to the Poynting vector ($\vec{S}\cdot\vec{k}'>0$), so light propagation in these composites is different from that reported for left-handed materials despite the fact that negative refraction can take place at the interface between air and both kinds of composites. However, wave coupling at the interfaces is well explained using the reduced wave vector ($\vec{k}$) in the first Brillouin zone, which is opposed to the energy flow, and agrees well with previous works dealing with negative refraction in photonic crystals.

OCIS codes: (160.4670) Optical materials; (260.2110) Electromagnetic theory.

References and Links

1. V. G. Veselago, "The electrodynamics of substances with simultaneously negative values of ε and μ," Sov. Phys. Usp. **10**, 509-514 (1968).
2. R. A. Shelby, D. R. Smith, and S. Schultz, "Experimental verification of a negative index of refraction," Science **292**, 77-79 (2001).
3. J. B. Pendry, A. J. Holden, W. J. Stewart, and I. Youngs, "Extremely Low Frequency Plasmons in Metallic Mesostructures," Phys. Rev. Lett. **76**, 4773-4776 (1996).
4. J. B. Pendry, A. J. Holden, D. J. Robbins, and W. J. Stewart, "Magnetism from Conductors and Enhanced Nonlinear Phenomena," IEEE Trans. Microwave Tech. **47**, 2075-2084 (1999).
5. N. García and M. Nieto-Vesperinas, "Is there an experimental verification of a negative index of refraction yet?," Opt. Lett. **27**, 885-887 (2002).
6. C. G. Parazzoli, R. B. Greegor, K. Li, B. E.C. Koltenbah, and M. Tanielian, "Experimental Verification and Simulation of Negative Index of Refraction Using Snell's Law," Phys. Rev. Lett. **90**, 107401 (2003); A. A. Houck, J.B. Brock, and I.L. Chuang, "Experimental Observations of a Left-Handed Material That Obeys Snell's Law," Phys. Rev. Lett. **90**, 137401 (2003).
7. J. D. Joannopoulos, P. Villeneuve, and S. Fan, "Photonic crystals: putting a new twist on light," Nature (London) **386**, 143-149 (1997).
8. H. Kosaka, T. Kawashima, A. Tomita, M. Notomi, T. Tamamura, T. Sato, and S. Kawakami, "Superprism phenomena in photonic crystals," Phys. Rev. B **58**, 10096-10099 (1998).
9. M. Notomi, "Theory of light propagation in strongly modulated photonic crystals: Refractionlike behavior in the vicinity of the photonic band gap," Phys. Rev. B **62**, 10696–10705 (2000).
10. S. Foteinopoulou and C. M. Soukoulis, "Negative refraction and left-handed behavior in two-dimensional photonic crystals," Phys. Rev. B **67**, 235107 (2003).
11. A. Martínez, H. Míguez, A. Griol, and J. Martí, "Experimental and theoretical study of the self-focusing of light by a photonic crystal lens," Phys. Rev. B **69**, 165119 (2004).

#7145 - $15.00 US Received 13 April 2005; revised 18 May 2005; accepted 19 May 2005

12. P.V. Parimi, W.T. Lu, P. Vodo, J. Sokoloff, J. S. Derov, and S. Sridhar, "Negative Refraction and Left-Handed Electromagnetism in Microwave Photonic Crystals," Phys. Rev. Lett. **92**, 127401 (2004).
13. B. Gralak, S. Enoch, and G. Tayeb, "Anomalous refractive properties of photonic crystals," J. Opt. Soc. Amer. A **17**, 1012-1020 (2000).
14. C. Luo, S. G. Johnson, J. D. Joannopoulos, and J. B. Pendry, "All-angle negative refraction without negative effective index," Phys. Rev. B **65**, 201104 (2002).
15. E. Cubukcu, K. Aydin, E. Ozbay, S. Foteinopoulou, and C. M. Soukoulis, "Negative refraction by photonic crystals," Nature (London) **423**, 604-605 (2003).
16. H.-T. Chien, H.-T. Tang, C.-H. Kuo, C.-C. Chen, and Z. Ye, "Directed diffraction without negative refraction," Phys. Rev. B **70**, 113101 (2004).
17. S. G. Johnson and J. D. Joannopoulos, "Block-iterative frequency-domain methods for Maxwell's equations in a planewave basis," Opt. Express **8,** 173-190 (2001), http://www.opticsexpress.org/abstract.cfm?URI=OPEX-8-3-173.
18. A. Taflove, *Computational Electrodynamics—The Finite Difference Time-Domain Method* (Artech House, Boston, 1995).
19. J. P. Berenger, "A Perfectly Matched Layer for the Absorption of Electromagnetic Waves," J. Comput. Phys. **114**, 185-200 (1994).
20. P. F. Loschialpo, D. L. Smith, D. W. Forester, F. J. Rachford, and J. Schelleng, "Electromagnetic waves focused by a negative-index planar lens," Phys. Rev. E **67**, 025602 (2003).
21. R.W. Ziolkowski and E. Heyman, "Wave propagation in media having negative permittivity and permeability," Phys. Rev. E **64**, 056625 (2001).
22. M. Qiu, L. Thylén, M. Swillo, and B. Jaskorzynska, "Wave propagation through a photonic crystal in a negative phase refractive-index region," IEEE J. Sel. Top. Quantum Electron. **9**, 106-110 (2003).
23. K. Sakoda, *Optical properties of photonic crystals* (Springer, Berlin, 2001).
24. A. Yariv, P. Yeh, *Optical Waves in Crystals : Propagation and Control of Laser Radiation* (New York, Wiley, 1984).

1. Introduction

In 1968, Soviet physicist Veselago analyzed theoretically the electromagnetic properties of media in which the real part of the magnetic permeability μ and the electric permittivity ε were both negative [1]. Veselago deduced that in this kind of medium the electric field $\vec{E}$, the magnetic field $\vec{H}$ and the wave vector $\vec{k}$ would form a left-handed set of vectors (this is the reason why these media are usually known as left-handed materials, LHMs), which means that the wave vector and the Poynting vector $\vec{S}$ are antiparallel ($\vec{S}\cdot\vec{k}<0$) and the phase velocity is opposite to the energy flow. This particular property would give rise to unexpected phenomena such as negative refraction at the interface between air and an LHM, focusing of electromagnetic radiation by a negative-index flat plate, reversed Doppler effect and reversed Cerenkov radiation [1]. Although Veselago also suggested some ways about how to construct a real LHM, it has been more than 30 years after that LHMs have been demonstrated experimentally [2]. Following the work of Pendry and coworkers [3,4], a composite structure consisting of square metallic split-ring resonators and wire strips was demonstrated to refract negatively (that is, to the same side of the normal to the interface) the electromagnetic waves impinging from free space to the LHM [2]. Although there was a debate (see [5], for instance) about the right interpretation of the experimental results reported in Ref. 2, more recent works have demonstrated that the composite described above follows the Snell's law provided that a negative effective index is associated to the LHM [6].

Other materials that have shown to refract negatively the electromagnetic radiation are photonic crystals (PhCs) [7]. One of the advantages of negative refraction in PhCs compared to the LHMs described above is that PhCs can be properly scaled in space to work at any frequency range, for example, infrared or visible wavelengths, if the materials are properly chosen. In a PhC the permitivitty ε is always locally positive whereas the permeability is μ = 1. Electromagnetic propagation inside a PhC takes place in the form of Bloch waves governed by the dispersion diagram that relates the frequency and the wave vector for each electromagnetic mode. One of the most interesting properties of PhCs is the existence of certain frequency intervals, commonly known as photonic band gaps, in which wave propagation is forbidden regardless of the wave vector. PhCs have also very interesting

#7145 - $15.00 US Received 13 April 2005; revised 18 May 2005; accepted 19 May 2005

properties as photonic conductors, one of them being their ability to deflect the electromagnetic radiation in the "wrong" way as it occurs in a LHM [8]. At this point, let us stress that the propagation of electromagnetic waves inside a PhC is a consequence of the multiple diffraction through the strongly-modulated periodic lattice of dielectric scatterers, which can give rise to extraordinary physical phenomena such as that studied in this paper, i. e., the so-called negative refraction. Notomi [9] showed that PhCs can behave as dielectric materials with an effective index of refraction in certain spectral regions where the equifrequency surfaces (EFSs) become rounded, despite of the fact that the underlying physical phenomenon is not really refraction. If the EFS shrinks with increasing frequency then the group velocity points inwards and a phenomenon of negative refraction can be expected at the interface between the PhC and air [9]. This is the case analyzed throughout this paper, in which the term "refractive" will be used to describe the studied phenomenon since it has been widely used in the literature.

Negative refraction in a PhC was first observed experimentally at optical frequencies by Kosaka *et al* [8]. Other authors have realized theoretical studies about the conditions under which negative refraction occurs in PhCs [9-10]. Recently, the experimental demonstration of negative refraction in a two-dimensional (2D) PhC working at microwave frequencies has also been reported [11-12]. It should be noticed that it has been reported that negative refraction in PhCs can also occur at frequencies in the first photonic band [13-15]. In this case, an effective index of refraction cannot be associated to the PhC since the corresponding EFSs do not become rounded and the observed negative deflection of the beam inside the PhC can be explained by considering that the existence of a pseudogap for one of the two main symmetry directions makes the waves to travel along the allowed direction, which in some cases can be confused with negative refraction [16]. In fact, in this case the wave is not refracted negatively in the wedge's experiment [2], as reported in Ref. 10. This phenomenon will not be considered here.

In this paper we intend to shed more light in the phenomenon of negative refraction in PhCs. To this end, the evolution of the phase fronts of a wave propagating inside a PhC is analyzed in a frequency region in which the PhC can be considered as an effective medium in which negative refraction takes place at the interface air-PhC [9]. Surprisingly, we find that, in contrast with conventional LHMs in which the phase fronts advance is opposite to the energy flow, in a PhC both the phase velocity (defined for the plane wave component of the Bloch mode with the largest amplitude) and the energy flow (parallel to the group velocity in an infinite PhC) point in the same direction, both away from the source. We will see that this behavior can be explained by considering the excitation of states with wave vectors out of the first Brillouin zone that carry the main part of the Bloch wave energy. Despite this fact, negative refraction occurs at the interface between the PhC and air because of the existence of another plane wave component whose wave vector is inside the first Brillouin zone and is opposed to the energy flow inside the PhC. The refracted angles can be predicted with quite good accuracy by means of the Snell's law with a negative effective index associated to the wave vector inside the first Brillouin zone, as in the case of LHMs.

2. Negative refraction at the interface between a 2D PhC wedge and air

In our study, we work with a 2D PhC made of dielectric rods with $\varepsilon = 10.3$ and radius $r = 0.4a$, a being the lattice constant, arranged in a triangular lattice. The results shown here can be easily extended to other types of 2D as well as three dimensional PhCs. We use a plane wave expansion method [17] to calculate the band diagram of this PhC for TM polarization (electric field parallel to the rods' axis). This band diagram is shown in Fig. 1(a). Frequency is represented in normalized units fa/c, f being the absolute frequency and c the light speed in vacuum. We will pay special attention to the two first frequency bands, highlighted in Fig. 1(a) as 1 and 2. For both bands there are frequency intervals for which the EFSs in the reciprocal space are circles. In these regions the PhC behaves as an isotropic dielectric material to which an effective refractive index n_{eff} that can be obtained from the radius of the corresponding EFS at each frequency can be associated [9]. Figures 1(b) and 1(c) show n_{eff} for

#7145 - $15.00 US Received 13 April 2005; revised 18 May 2005; accepted 19 May 2005

the bands 1 and 2 respectively calculated as explained in Ref. 10 for ΓM and ΓK directions. The sign of n_{eff} is positive if the radius of the EFS grows with increasing frequency and negative in case it shrinks [9]. The refractionlike behavior is evident when n_{eff} is identical for both ΓM and ΓK directions. For example, at the frequency 0.15 (first band) the PhC behaves as an effective medium with n_{eff} = 2.588. The same occurs in the second band for frequencies above 0.33. Following the results of Refs. 9 and 10 it could be expected that for frequencies in the second band the phase velocity and the group velocity are antiparallel and waves that travelling through free space impinge in this PhC should be negatively refracted with an angle that can be predicted from the Snell's law using the effective index plotted in Fig. 1(c).

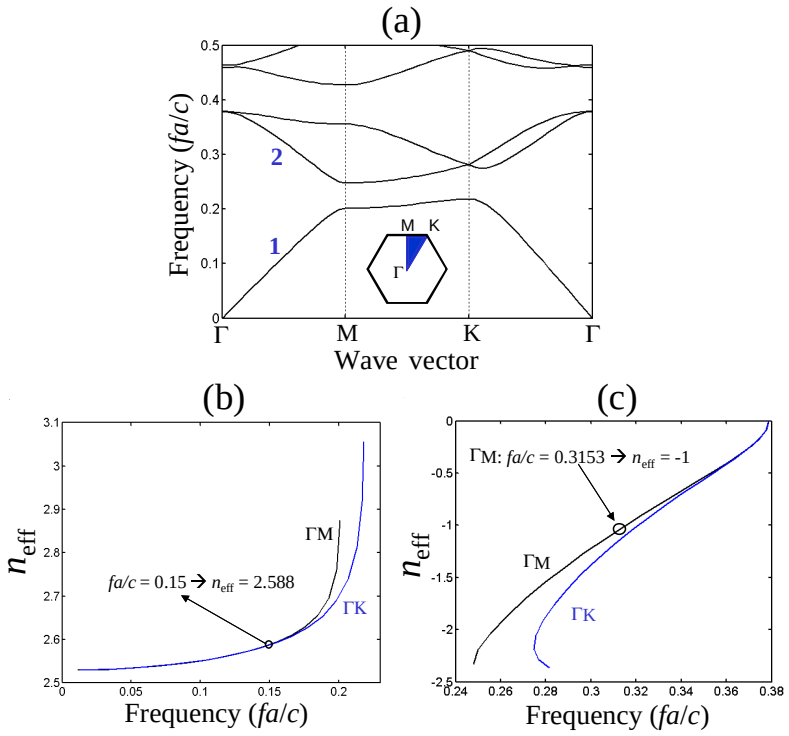

Fig. 1. (a) TM-polarization photonic band structure of the 2D PhC under study: a triangular lattice (the inset shows its first BZ) of dielectric rods with ε = 10.3 and radius r = 0.4a. Effective refractive index n_{eff} of (b) the first and (c) the second photonic bands for the ΓM and ΓK directions of propagation.

To demonstrate the negative refraction behavior we simulate the wedge experiment reported in Refs. 2, 6, 10 and 12 using the finite-difference time-domain (FDTD) method [18] with perfectly-matched layer boundary conditions [19]. The first air-PhC interface is chosen to be along the ΓK direction (so the interface normal is parallel to the ΓM direction). Then the wave propagation inside the PhC is along the ΓM direction for which the modes corresponding to the first two bands have an even symmetry, which makes easier the excitation of the Bloch modes by an external plane wave. Figures 2(a) and 2(b) represent the propagation of the TM-polarized electric field through the wedge structure obtained from FDTD calculations for two different output interfaces (highlighted with the bold solid lines in Figs. 2(a) and (b)): (a) along ΓK, and (b) along ΓM. The frequency of the wave is fa/c = 0.3153, so n_{eff} = -1 for propagation along ΓM. As it is shown in Fig. 1(c), n_{eff} is slightly different for ΓM (n_{eff} = -1) and ΓK (n_{eff} = -1.15) at the frequency 0.3153. This means that the EFS is a hexagon-like circle, not really a circle. However, this fact has almost no influence on

#7145 - $15.00 US
Received 13 April 2005; revised 18 May 2005; accepted 19 May 2005

the study carried out in this paper. The reason to choose such a frequency is that the EFS of the PhC is almost the same that for free space propagation, so the analysis to be carried out is more straightforward. The incident angles with respect to the normal (dashed lines in Figs. 2(a) and (b)) to the output interfaces are respectively ϕ_{i1} = 60º (Fig. 2(a)) and ϕ_{i2} = 30º (Fig. 2(b)). It is observed that refraction occurs to the same side of the interface normal and there is only a single ray propagating outside the PhC. The refracted angles can be roughly estimated from the phase fronts of the waves in free space and they are close to the values ϕ_{r1} = -60º (Fig. 2(a)) and ϕ_{r2} = -30º (Fig. 2(b)) that can be obtained by applying the Snell's law with a negative effective index at the PhC side. From these results and taking into account previous works, one might conclude that inside the PhC the wave propagates backwards (in the sense of the evolution of the phase fronts) and opposed to the energy flow, as in a LHM, and that when the wave reaches the output interface the wave vector component normal to the surface changes its sign so negative refraction takes place. The next section is devoted to deeply analyze the wave propagation in the bulk of the PhC.

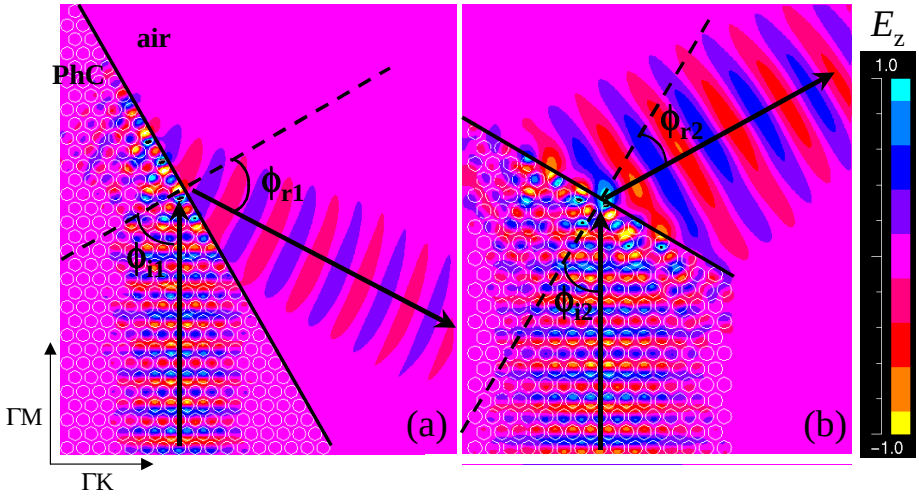

Fig. 2. FDTD simulation of the refraction of a monochromatic wave (*fa*/*c* = 0.3153) that propagates along the ΓM direction in a 2D PhC wedge. The output interface is along (a) ΓM and (b) ΓK directions. The electric field parallel to the rods' axis is shown. The output PhC-air interface is highlighted with a bold solid line. The normal to the interface is highlighted with a bold dashed line. Arrows show the propagation direction of the waves inside the PhC and in air.

3. Wave propagation inside a photonic crystal in a region with a negative effective index of refraction

To study wave propagation inside the PhC we consider a semi-infinite PhC like the studied above with rectangular instead of wedge shape in which a monochromatic TM-polarized wave is injected. The input interface is along the ΓK direction as in the wedge's type calculations and the wave propagates along the ΓM direction. One lattice constant after the input interface we place a series of 101 electric field monitors (the field component parallel to the rods is measured) along the ΓM direction with a spacing of $\sqrt{3}a/20$ between them and centered with respect to the symmetry axis of the incident wave in order to spatially sample the wave in the propagation direction. We make the PhC large enough in the propagation direction (more than 40 periods along the ΓM direction) in order to ensure that the reflected wave does not modify the monitored fields (the simulations end before the reflected wave reaches the monitors). In other words, we can say that our PhC is semi-infinite in the sense that only the wave that propagates away from the source is considered in the analysis. We present the results as in Ref. 20: a diagram that represents the electric field amplitude with the simulation time in the

#7145 - $15.00 US
Received 13 April 2005; revised 18 May 2005; accepted 19 May 2005

vertical direction (in ct/a units, t being the absolute time) and the space (monitor position) in the horizontal direction. This kind of diagram allows a straightforward visualization of the phase fronts, as shown in Fig. 3 where the time-spatial evolution of an electromagnetic wave is presented for three different cases: (a) free-space propagation with fa/c = 0.3153, (b) propagation inside the PhC for fa/c = 0.15 (first band); and (c) propagation inside the PhC for fa/c = 0.3153 (second band). From Fig. 3 we can state that only in the case of free-space propagation (Fig. 3(a)) the phase fronts (lines with the same color in the diagrams) can be easily identified as they correspond to a plane wave. The phase velocity can be estimated from the slope of the phase fronts and is approximately equal to c, as expected. However, for the cases of propagation inside the PhC (Figs. 3(b) and (c)) a periodic modulation of the phase fronts is observed, as the wave inside the PhC is a Bloch mode that can be expressed as a set of plane waves. It is not easy to associate a phase index from these diagrams, owing to the modulation of the field, but what is really surprising is that the behavior of the wave inside the PhC is very similar for both bands 1 (positive index) and 2 (negative index), discounting the fact that the modulation is stronger for the second band. Moreover, from Fig. 3(c) we can see that the modulated phase fronts have a positive slope, in clear contrast to the diagram shown in Ref. 20 for a LHM. If we consider the main phase front (this concept will be analyzed more in detail in the next section), highlighted with a dashed line in Figs. 3(b) and (c) and corresponding to the main plane wave component that forms the Bloch wave, it travels upwards in the direction of the energy flow. Similar results were observed for other frequencies corresponding to the first and second band and employing a different spacing between field monitors, and backward-wave propagation was not identified in any case. We also tried to estimate the group velocity v_g for each case from the slope of the leading edge of the monochromatic wave as shown by the bold solid line that forms an angle α with respect to the horizontal in Fig. 3(c). The results so obtained ($v_g = 0.345c$ at fa/c = 0.15 and $v_g = 0.276c$ at fa/c = 0.3153) were in excellent agreement with the group velocities ($v_g = 0.362c$ at fa/c = 0.15 and $v_g = 0.294c$ at fa/c = 0.3153) obtained from the band diagram (infinite PhC).

The detected electric field for two adjacent field monitors (numbers 50 and 51, specifically) is shown in Figs. 4(a)-(d), as in Ref. [21]. Figures 4(a) and 4(b) correspond to the frequency 0.15 whereas Figs. 4(c) and 4(d) are obtained for the frequency 0.3153. The left-side diagrams shows the time step when the edge of the incoming wave reaches the monitors whereas the right-side ones show a time interval of the field once the steady state has been approximately reached (we can assume that the wave is monochromatic). As expected from causality considerations, in both cases the wave reaches the first monitor before than the second (see Figs. 4(a) and 4(c)). We also find that the phase front reaches before the monitor 50 than the monitor 51 when the steady state has been achieved regardless of the frequency (and, therefore, the sign of n_{eff}). The results shown in Fig. 4(d) are in clear disagreement with what would be expected for a LHM, in which the phase fronts would reach first the monitor 51 [21]. Similar diagrams (not shown here) were obtained by choosing other adjacent field monitors.

#7145 - $15.00 US Received 13 April 2005; revised 18 May 2005; accepted 19 May 2005

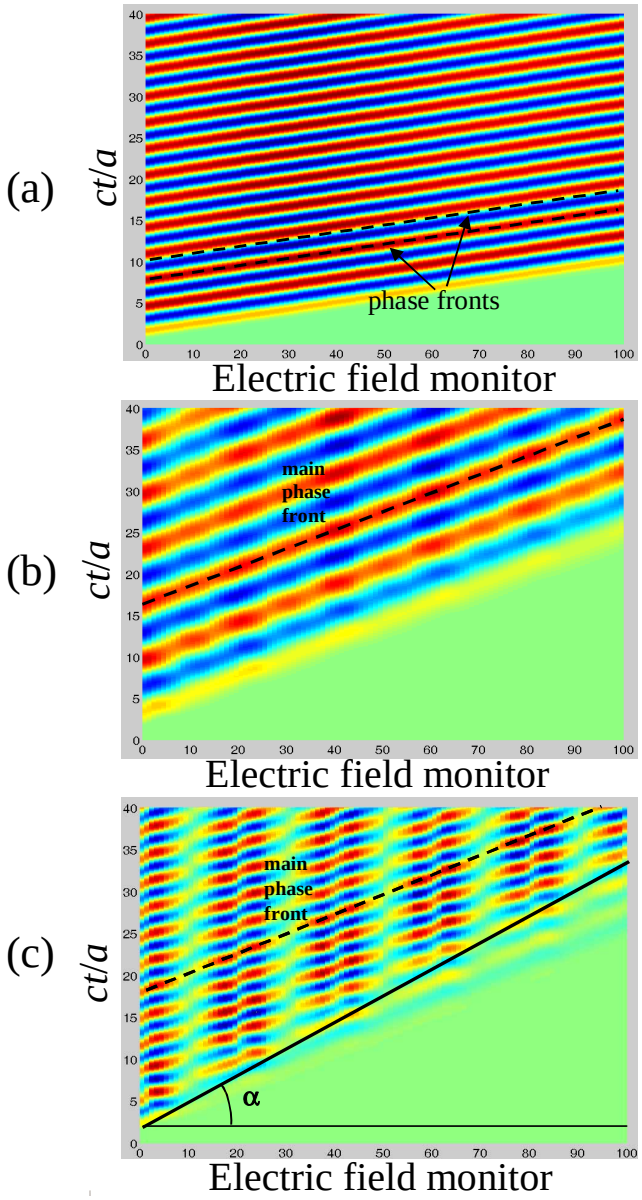

Fig. 3. Diagrams showing the evolution of the electric field with time (vertical axis) and space (horizontal axis). 101 field monitors are employed in a 2D FDTD simulation. In all cases the wave is monochromatic and TM-polarized. (a) Propagation in air, *fa/c* = 0.3153; (b) Propagation inside the PhC described in Fig. 1, *fa/c* = 0.15, (c) Propagation inside the PhC described in Fig. 1, *fa/c* = 0.3153. The phase fronts are the lines of the same color and the inverse of their slope gives the phase velocity. The slope of the arriving impulse stands for the group velocity, which can be obtained from the angle α in Fig. 3(c). The dashed lines in (b) and (c) highlight the slope of the main phase front.

#7145 - $15.00 US
Received 13 April 2005; revised 18 May 2005; accepted 19 May 2005

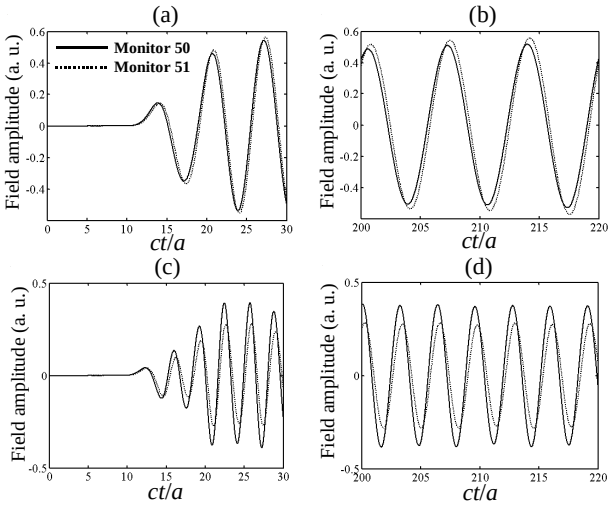

Fig. 4. Detected electric field at the field monitors 50 and 51 (spaced $\sqrt{3}a/20$ along the ΓM direction). A TM-polarized monochromatic wave propagating along ΓM and with frequencies fa/c = 0.15 [(a) and (b)] and 0.3153 [(c) and (d)] is injected in the 2D PhC. The diagrams (a) and (c) corresponds to the arrival of the leading edge (related to the group velocity). The diagrams (b) and (d) correspond to a time step for which the steady state has been reached and the signal can be considered almost monochromatic (related to the phase velocity).

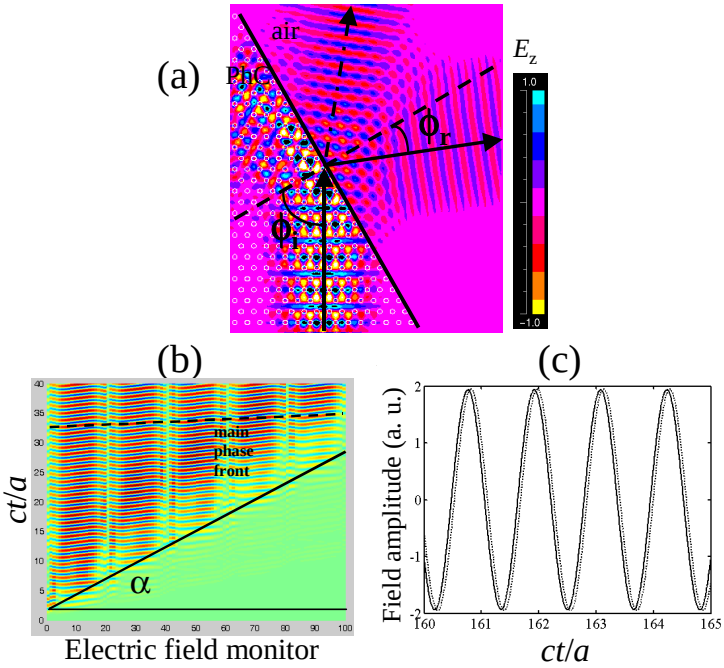

Fig. 5. Study of the 2D PhC in Ref. 11: a triangular lattice of dielectric rods (r = 0.182 and ε = 11), fa/c = 0.8648. (a) FDTD simulation (electric field) of the refraction of a monochromatic wave that propagates along the ΓM direction in a 2D PhC wedge. Output interface along the ΓM direction. (b) Diagram showing the evolution of the electric field with time (vertical axis) and space (horizontal axis) inside the PhC. 101 field monitors are employed. (c) Detected electric field at the field monitors 50 and 51 (spaced $\sqrt{3}a/20$ along the ΓM direction).

#7145 - $15.00 US
Received 13 April 2005; revised 18 May 2005; accepted 19 May 2005

4. Plane-wave decomposition of a Bloch mode that propagates inside a 2D PhC

A TM-polarized Bloch mode that propagates inside a 2D PhC can be written as a superposition of plane waves as follows [23]:

$$E_z(\vec{r},\vec{k}) = \sum_{m=-\infty}^{\infty}\sum_{n=-\infty}^{\infty} E_{m,n}\exp\left[j(\vec{k}+m\vec{G}_1+n\vec{G}_2)\right] \qquad (1)$$

where the sum applies to all the vectors on the 2D reciprocal space ($\vec{G} = m\vec{G}_1 + n\vec{G}_2$, m and n being integers), $E_{m,n}$ is the electric field amplitude of the component with wave vector $\vec{k}+m\vec{G}_1+n\vec{G}_2$, and $\vec{k}$ is the wave vector in the first BZ or fundamental wave vector. In a triangular lattice the vectors $\vec{G}_1$ and $\vec{G}_2$ can be chosen as $\vec{G}_1 = \frac{2\pi}{a}(\hat{x}+\frac{1}{\sqrt{3}}\hat{y})$ and $\vec{G}_2 = \frac{2\pi}{a}(-\hat{x}+\frac{1}{\sqrt{3}}\hat{y})$, where $\hat{x}$ and $\hat{y}$ are the unit vectors in the ΓK (transverse) and the ΓM (longitudinal) directions, respectively (see Fig. 6). It should be noticed that although $\vec{k}$ is the fundamental wave vector, this fact does not necessarily imply that the plane wave with wave vector $\vec{k}$ carries most of the Bloch wave energy. In other words, $E_{0,0} > E_{m,n}$ for $m \neq 0$, $n \neq 0$, is not mandatory.

Suppose we inject a TM-polarized monochromatic plane wave with frequency fa/c = 0.3153 propagating through air into the 2D PhC previously analyzed (see Fig. 1). The interface is along ΓK, as in Fig. 2(a), and the incidence is normal to the surface, so the propagation inside the PhC is along ΓM. At the chosen frequency, the EFSs of the air and the 2D PhC are almost identical, although in the PhC the EFS is replicated on the whole reciprocal space due to the 2D periodicity of the structure. When the wave enters the 2D PhC the normal component of the incident wave vector [$\vec{k}_i = 0.315(2\pi/a)\hat{y}$ in Fig. 6] should reverse its sign since we are in a region in which the EFS of the PhC is identical to that of the air but with the group velocity pointing inwards [1,9-10]. The boundary conditions at the interface impose that [8]

$$k_{PhC//} = k_{i//} + 2\pi l/a \qquad (2)$$

with $k_{i//}$ and $k_{PhC//}$ being the wave vector components parallel to the interface in air and inside the 2D PhC respectively, a the periodicity of the interface along ΓK (that in this case is the lattice constant) and l an integer. As the incidence is normal to the interface, we have $k_{i//} = 0$ so $k_{PhC//} = 2\pi l/a$.

In agreement with the band diagram shown in Fig. 1(a) and the refraction results shown in Fig. 2, we can conclude that the fundamental wave vector of the Bloch mode is $\vec{k}_{0,0} = -0.315(2\pi/a)\hat{y}$ (see Fig. 6), as at this point the group velocity, and therefore, the energy flow, points upwards so causality is not violated [9-10]. However, this is not the only wave vector that forms the Bloch wave. Instead, the Bloch wave has the form of Eq. (1) with fundamental wave vector $\vec{k} = \vec{k}_{0,0} = -0.315(2\pi/a)\hat{y}$. In the following study we will only take into account the seven wave vectors of first-order, that is, $\vec{k}_{m,n} = \vec{k}_{0,0} + m\vec{G}_1 + n\vec{G}_2$ with $|m|, |n| \leq 1$ (see Fig. 6). Since we are analyzing the second band we think that the results obtained taking into account only this set of wave vectors can be enough to give a good picture of the propagation inside the PhC.

#7145 - $15.00 US Received 13 April 2005; revised 18 May 2005; accepted 19 May 2005

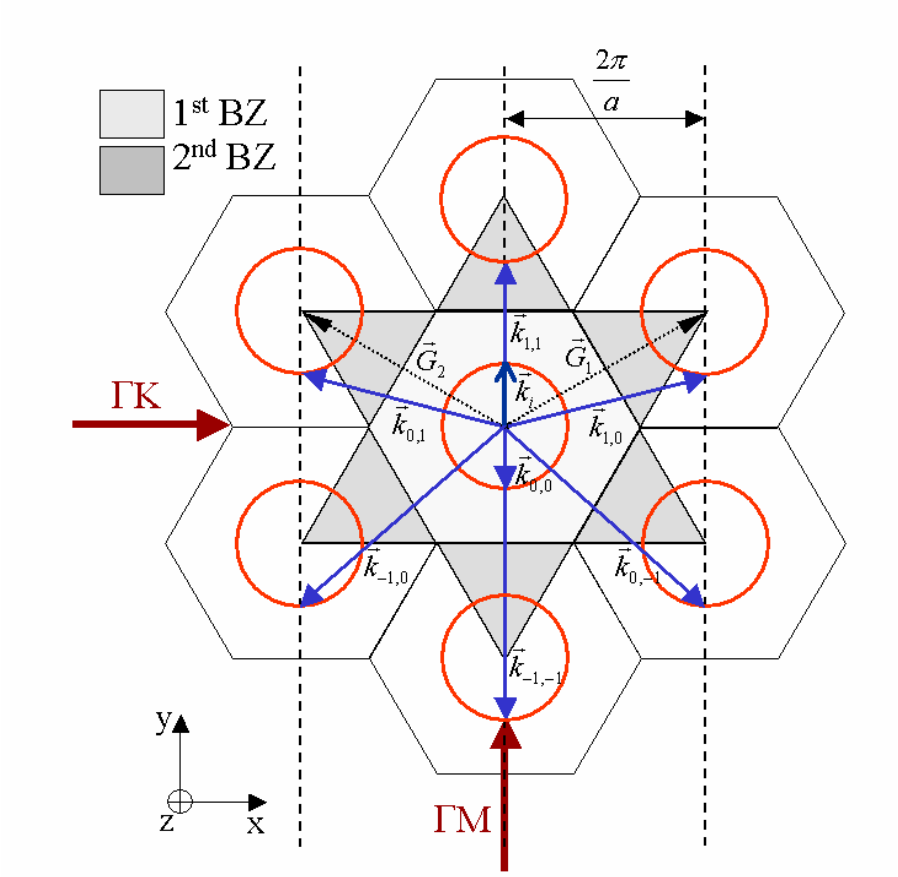

Fig. 6. Wave vector diagram of the 2D PhC under study (Fig. 1). The red circular contours correspond to the EFSs at frequency fa/c = 0.3153. The fundamental vectors of the reciprocal lattice are $\vec{G}_1$ and $\vec{G}_2$. First and second BZs are highlighted with different gray tones.

The field amplitude $E_{m,n}$ of each plane wave is obtained by use of the space sampling of the electric field propagated inside the PhC: a sampling of the electric field along the ΓM (ΓK) directions permits to obtain the wave vectors along the y (x) direction and an estimation of the field amplitude of the plane wave with such a wave vector component. First, we perform a transverse sampling with 51 electric field monitors spaced a/20 (in the transverse direction, ΓK, the period is a), the first monitor placed on the mirror symmetry axis of the propagating signal. As observed in Figs. 2(a) and 2(b), the field has an even symmetry when propagates along ΓM at a frequency corresponding to the second band so we can double the number of samples when applying the Fourier transform. Then we choose a time step in which the steady state has been reached (as before, we consider a time step for which the wave can be assumed fully monochromatic) and calculate the space Fourier transform of the field monitored at each point in order to obtain information in the wave vector space. It should be mentioned that this procedure is just an estimation of the transverse electric-field composition as we are sampling only along a line (one-dimensional sampling) and not over the whole 2D space. The results for the transverse sampling are shown in Fig. 7(a). It should be noted that similar results were obtained for other time steps after the reaching of the steady state and also after displacing the field monitor half a period in the ΓM direction. As our FDTD calculations only allow us to obtain a measure of the amplitude but not the phase of the

#7145 - $15.00 US
Received 13 April 2005; revised 18 May 2005; accepted 19 May 2005

field, we cannot obtain information about the sign of the wave vectors. From Fig. 7(a) we can state that the main plane wave components have a zero wave vector in the *x* direction, as the 85.45 % of the power is carried by a zero transverse wave vector. In contrast, the power carried by plane waves with transverse wave vectors of absolute value $2\pi/a$ is only about the 12.6 % of the total power. These components are responsible for the transverse periodic modulation of the wave that is observed in Figs. 2(a) and 2(b). It should be mentioned that we estimate the power of each component as the sum of the squares of each field component.

The same analysis is done with the field monitors along the propagation (longitudinal) direction. In this case we place 201 field monitors spaced $\sqrt{3}a/40$ and also take the Fourier transform of the sampled electric field at a given time step assuming that the wave has reached its steady state and no reflected waves are present. Similar results were also obtained at other time steps and also by displacing the monitors half a period rightwards. Figure 7(b) shows the obtained distribution of field amplitudes at each wave vector (in the propagation direction). We can appreciate clearly three main contributions with absolute (at previously stated, the sign of the wave vector cannot be estimated from our simulations) wave vectors $0.26(2\pi/a)$, $0.835(2\pi/a)$ and $1.46(2\pi/a)$ that carry about the 13 %, the 85 % and the 2 % of the total power, respectively. Comparing these results with the wave vector distribution shown in Fig. 6, we can relate the obtained contributions with the wave vectors $\vec{k}_{1,0} = 2\pi/a\hat{x} - 0.262(2\pi/a)\hat{y}$ (and its symmetric counterpart, $\vec{k}_{0,1} = -2\pi/a\hat{x} - 0.262(2\pi/a)\hat{y}$), $\vec{k}_{1,1} = 0.84(\pi/a)\hat{y}$, and $\vec{k}_{-1,-1} = -1.47(2\pi/a)\hat{y}$, respectively. Owing to the symmetry of the PhC, we can assume that both wave vectors, $\vec{k}_{1,0}$ and $\vec{k}_{0,1}$, are equally excited and, therefore, they carry the same power. Surprisingly, we do not find any wave vector with an absolute value close to $0.313(2\pi/a)$ that could be associated to fundamental component inside the first BZ, $\vec{k}_{0,0}$. One reason to explain this is that, owing to an insufficient sampling accuracy, the $\vec{k}_{0,0}$ component may be masked by the component $\vec{k}_{1,0}$ with a longitudinal component $0.26(2\pi/a)$. Then we repeated the procedure but with a spacing of $\sqrt{3}a/5$ between adjacent field monitors in order to be able to distinguish these two components. Figure 7(c) shows the distribution of field amplitudes at $fa/c = 0.3153$ but for different samplings: $\sqrt{3}a/20$ (solid curve) and $\sqrt{3}a/5$ (dashed curve). From Fig. 7(c) we can see that, although when the spacing between monitors is $\sqrt{3}a/20$ a unique peak appears around $0.25(2\pi/a)$, when the spacing is $\sqrt{3}a/5$ two different peaks are clearly discernible: one at $0.26(2\pi/a)$ that corresponds to $\vec{k}_{1,0} = 2\pi/a\hat{x} - 0.262(2\pi/a)\hat{y}$ as stated before, and another one at $0.315(2\pi/a)$ that corresponds to the fundamental wave vector $\vec{k}_{0,0} = -0.315(2\pi/a)\hat{y}$. However, we find that the amplitude of the field component with wave vector $\vec{k}_{0,0}$ is much lower than the amplitude of the other main components, $\vec{k}_{1,0}$ and $\vec{k}_{1,1}$. We pay special attention on the fact that for both the transversal and the longitudinal sampling we obtain that the total power carried out by components with transverse wave vector equal to $2\pi/a$, that is, $\vec{k}_{1,0}$ and $\vec{k}_{0,1}$, is about the 13 % of total power of the Bloch wave. The agreement between the EFS plot shown in Fig. 6 (in which the EFS radius is calculated from the band diagram) and the Fourier decomposition is excellent.

#7145 - $15.00 US Received 13 April 2005; revised 18 May 2005; accepted 19 May 2005

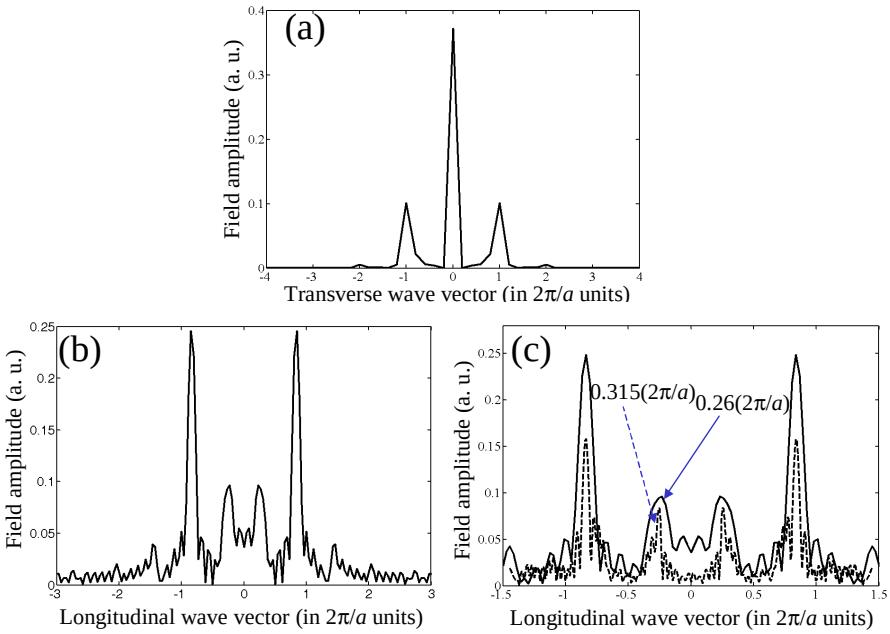

Fig. 7. Plane-wave decomposition of the space sampling of the electric field that propagates inside the PhC under study along the ΓM direction. The field correspond to a simulation time step for which the wave has reached its steady state. (a) Transverse sampling (a/20 spacing); (b) longitudinal sampling ($\sqrt{3}a/40$ spacing); (c) longitudinal sampling: $\sqrt{3}a/20$ spacing (solid curve) and $\sqrt{3}a/5$ spacing (dashed curve). The peaks corresponds to the amplitude of a certain plane wave component of the whole Bloch wave.

From the results depicted in Fig. 7 we can also state that the main plane-wave component of the Bloch wave propagation though the 2D PhC has a wave vector $\vec{k}_{1,1} = 0.84(2\pi/a)\hat{y}$, which is well outside the first BZ. Specifically, as shown in Fig. 6, it is located in the second BZ, as we could have deduced intuitively by considering that we are exciting the second photonic band. Moreover, if we associate a phase velocity to the plane wave with wave vector $\vec{k}_{1,1}$ we obtain that it corresponds to the main phase front component shown before with a dashed line in Fig. 3(c). And more surprisingly, we find that the main plane wave component is not a backward wave (the components corresponding to the backwards wave vectors $\vec{k}_{0,0}$ and $\vec{k}_{-1,-1}$ carry a small amount of power) as in a conventional LHM, but a forward one, with it phase front moving in the same direction that the energy flow. In this way, PhCs behave clearly in a different way than LHMs. In fact, we obtain that in PhCs it takes more sense to define the phase velocity as that of the main plane wave component, and not that of the fundamental component (inside the first BZ), paying attention to the evolution of phase fronts inside the PhC. This results agrees with that given in Ref. 24 when analyzing wave propagation in one dimensional periodic layered media. However, the value of n_{eff} to be used in the Snell's law to analyze wave refraction should be defined by choosing the fundamental wave vector.

The analysis described above has been applied to other frequencies in order to check and compare the previous results. The same procedure was employed but with a spacing of $\sqrt{3}a/20$ between adjacent field monitors. For example, Fig. 8(a) depicts the wave vector decomposition of the electric field when monochromatic waves with frequencies corresponding to the first band (fa/c = 0.1 and 0.15 respectively) are injected in our PhC. Only

#7145 - $15.00 US Received 13 April 2005; revised 18 May 2005; accepted 19 May 2005

positive wave vectors are shown to better appreciate the amplitude peaks. We can see that there is a unique relevant field component for each frequency and this component has a wave vector that agrees well with the wave vector inside the first BZ obtained from the band diagram: $\vec{k}_{0,0} = 0.25(2\pi/a)\hat{y}$ for *fa*/*c* = 0.1 and $\vec{k}_{0,0} = 0.39(2\pi/a)\hat{y}$ for *fa*/*c* = 0.15. Then, in clear contrast with the results shown previously in Fig. 7, we can state that for frequencies within the first band the plane wave component that carries almost all the power of the Bloch state is that with $\vec{k}_{0,0}$, which is inside the first BZ. This result agrees with the main phase front slope highlighted in Fig. 3(b) with a dashed line. The lack of other significant components in the plane wave decomposition also agrees with the slightly-modulated field shown in Fig. 3(b). This effect can be simply explained by the fact that at low frequencies the wavelength is much larger than the PhC periodicity and the wave sees an almost homogeneous medium so the wave that propagates inside the PhC mostly behaves as a plane wave with wave vector $\vec{k}_{0,0}$. In other words, at low frequencies the system is highly refractive. Figure 8(b) shows the same plane-wave decomposition but for frequencies corresponding to the second band: *fa*/*c* = 0.3, 0.33 and 0.36. In the three cases, we observe similar features to those previously analyzed for the frequency *fa*/*c* = 0.3153: i) the main plane wave component is that corresponding to a wave vector $\vec{k}_{1,1}$; ii) the existence of a component with wave vector $\vec{k}_{0,0}$ is noticed in Fig. 8(b) as the value of this wave vector should diminish with increasing frequency, in contrast to the $\vec{k}_{1,0}$ and $\vec{k}_{1,1}$ whose longitudinal components increase with frequency; and iii) the obtained wave vectors are in good agreement with those that can be obtained by replicating the fundamental wave vector $\vec{k}_{0,0}$ obtained from the band diagram on the reciprocal space as shown in Fig. 6. It is also interesting to notice that the amplitude of the component with wave vector $\vec{k}_{0,0}$ is very small compared to the components with wave vectors $\vec{k}_{1,0}$ and $\vec{k}_{1,1}$ at *fa*/*c* = 0.36.

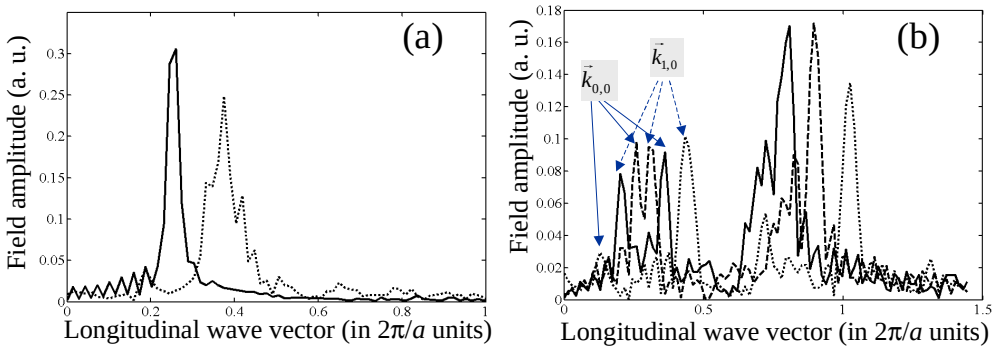

Fig. 8. Plane-wave decomposition of the longitudinal sampling ($\sqrt{3}a/20$ spacing) of the electric field that propagates inside the PhC under study along the ΓM direction. The field correspond to a simulation time step for which the wave has reached its steady state. (a) first band: *fa*/*c* = 0.1 (solid curve); *fa*/*c* = 0.15 (dotted curve); (b) second band: *fa*/*c* = 0.3 (solid curve); *fa*/*c* = 0.33 (dashed curve), *fa*/*c* = 0.36 (dotted curve). Only positive wave vectors are shown.

We repeated this analysis at a frequency of *fa*/*c* = 0.5 corresponding to the fifth band (with a positive index, as the first band) and in the decomposition we also found that the main plane wave components had wave vectors out of the first BZ. In this case we also obtained a time-space diagram (not shown here) as those depicted in Fig. 3 and the result was that the main phase front had also a positive slope as the rest of the cases considered in the text. We also calculated the plane wave decomposition (not shown here) for the case described in Fig.

#7145 - $15.00 US Received 13 April 2005; revised 18 May 2005; accepted 19 May 2005

5 [11]. We found more components than in the previous example, mainly because of the high frequency (fa/c = 0.8648), and the main plane wave components were those with a transverse wave vector $2\pi/a$. However, and in agreement with the previous case, we found that the amplitude of the component with wave vector $\vec{k}_{0,0}$ was much smaller than other components with wave vectors out of the first BZ.

To conclude this section, let us describe the physical phenomenon that occurs at the output interface in the wedge structure. A schematic plot of our explanation is shown in Figs. 9(a) and 9(b), for the interfaces along ΓK and ΓM respectively. When the wave reaches the interface, the component of the wave vectors parallel to the interface is conserved. This condition is established by the dashed lines in Figs. 9(a) and 9(b). These lines are parallel and the spacing between them depends on the periodicity of the interface. The wave vectors that propagate in air are given by the crossing of these lines with the EFS of air, which, as we mentioned previously, coincides with that of the PhC, although in this case, as the air is an homogeneous medium, the EFS is not replicated on the reciprocal space. First let us discuss the case the case in which the output interface is along ΓK direction [see Fig. 9(a)]. The incident angle is ϕ_{i1} = 60º as in Fig. 2(a). Only the main wave vectors that contribute to the propagating the whole Bloch wave are plotted. From these $\vec{k}_{0,0}$ and $\vec{k}_{1,0}$ are the ones whose component parallel to the interface intersects with the air EFS. Both components give rise to the same refracted ray with wave vector $\vec{k}_r$. The direction of the energy flow in air points to the same direction than $\vec{k}_r$ and is given by the arrow in Fig. 9(a), in fairly agreement with the field distribution shown in Fig. 2(a).

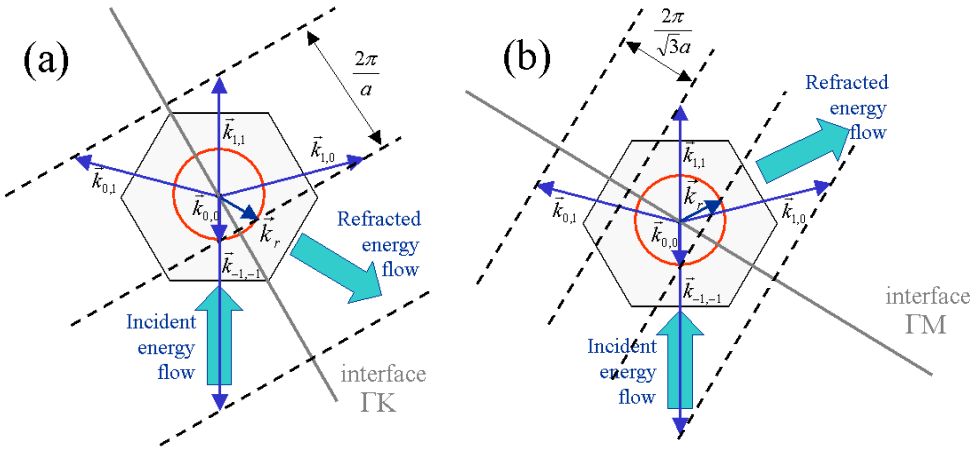

Fig. 9. Schematic explanation of the refraction at the output PhC-air interface using a wave vector diagram. The circle corresponds to the EFS of air. The hexagon is the first BZ of the PhC. The bold solid gray lines show the interface: (a) along ΓK; (b) along ΓM. The dashed lines represent the condition of conservation of the wave vector components parallel to the interface. The arrows stand for the energy flow of the wave before and after the interface.

The situation is slightly different when the interface is along ΓM [see Fig. 9(b)] since in this case $\vec{k}_{0,0}$ is the only wave vector having a component parallel to the interface that intersects the air EFS. The refracted ray with wave vector $\vec{k}_r$ obtained from this intersection, as depicted in Fig. 9(b), defines the direction of the refracted energy flow in air, in perfect agreement with the result in Fig. 2(b). The rest of components, $\vec{k}_{0,1}, \vec{k}_{1,0}$ and $\vec{k}_{1,1}$, which carry the main part of the energy of the Bloch wave propagating through the PhC, do not produce

#7145 - $15.00 US
Received 13 April 2005; revised 18 May 2005; accepted 19 May 2005

any intersection with the air EFS. An issue to be solved in a future work is to understand the behavior of the components with wave vectors $\vec{k}_{0,1}, \vec{k}_{1,0}$ and $\vec{k}_{1,1}$ when they reach the interface. The possible choices are: (i) these components are totally reflected at the interface since they are below the air light cone; (ii) these components transfer their energy to the $\vec{k}_{0,0}$ component so they can cross the interface and be refracted into air.

5. Conclusion

This work has analyzed the wave propagation inside a 2D PhC in a frequency regime for which negative refraction at the interface between the PhC and air occurs. We have shown that the angle of the refracted wave can be well explained using the wave vector inside the first BZ, as reported in previous works. However, we have found that the wave propagation inside the PhC with negative effective index n_{eff} is strongly different from the propagation inside a left-handed material in which the phase fronts evolve in the opposite direction of the energy flow. It is concluded that the main difference comes from the fact that in bulk of the PhC, the electromagnetic energy propagates in the form of a Bloch wave. It has been shown that at the frequency in which negative refraction occurs, the main component of the Bloch wave is a plane wave whose wave vector is outside the first BZ and that propagates in the same direction that the energy flow. In this sense, PhCs present a very different behavior in comparison to conventional LHMs, although negative refraction takes place for both kinds of composites.

Acknowledgments

This work has been partially funded by the Spanish Ministry of Science and Technology under grant TIC2002-01553.

#7145 - $15.00 US Received 13 April 2005; revised 18 May 2005; accepted 19 May 2005